

Shell-model phenomenology of low-momentum interactions

Achim Schwenk^{1,*} and Andrés P. Zuker^{2,†}

¹*Nuclear Theory Center, Indiana University, 2401 Milo B. Sampson Ln, Bloomington, IN 47408*
²*Institut de Recherches Subatomiques, IN2P3-CNRS, Université Louis Pasteur, F-67037 Strasbourg*

The first detailed comparison of the low-momentum interaction $V_{\text{low } k}$ with G matrices is presented. We use overlaps to measure quantitatively the similarity of shell-model matrix elements for different cutoffs and oscillator frequencies. Over a wide range, all sets of $V_{\text{low } k}$ matrix elements can be approximately obtained from a universal set by a simple scaling. In an oscillator mean-field approach, $V_{\text{low } k}$ reproduces satisfactorily many features of the single-particle and single-hole spectra on closed-shell nuclei, in particular through remarkably good splittings between spin-orbit partners on top of harmonic oscillator closures. The main deficiencies of pure two-nucleon interactions are associated with binding energies and with the failure to ensure magicity for the extruder-intruder closures. Here, calculations including three-nucleon interactions are most needed. $V_{\text{low } k}$ makes it possible to define directly a meaningful unperturbed monopole Hamiltonian, for which the inclusion of three-nucleon forces is tractable.

PACS numbers: 21.60.Cs, 21.30.+x, 21.10.-k

Microscopic nuclear structure studies fall in three categories. For local interactions, the Green's Function Monte Carlo (GFMC) method [1, 2] leads to exact solutions of the many-body Schrödinger equation by evaluation of multi-dimensional integrals in coordinate space. The No-Core Shell-Model (NCSM) [3, 4] relies on matrix diagonalizations in a harmonic oscillator basis of $N\hbar\omega$ excitations with respect to a minimal $0\hbar\omega$ space. Convergence with $N\hbar\omega$ is slow for conventional nucleon-nucleon (NN) interactions, which are replaced by effective interactions that are model-space dependent. Both GFMC and converged NCSM methods are limited at present to mass number $A \lesssim 12$. The standard Shell-Model (SM) [5] restricts diagonalizations to $0\hbar\omega$ spaces and treats higher excitations in perturbation theory. It bypasses saturation problems by using a G matrix [6] calculated at approximately the experimental nuclear radius ($\hbar\omega \approx 40A^{-1/3}$) and uses experimental single-particle energies. Presently, exact SM diagonalizations are possible for all semi-magic nuclei, and for $A < 70$ in full $0\hbar\omega$ spaces.

It has been traditionally assumed that NN interactions are strongly repulsive at short distances, and therefore require resummations to obtain “pseudopotentials” in a given model space. For fifty years the standard in nuclear physics has been the Brueckner-Bethe-Goldstone G matrix, which is calculated from a NN potential V by summing two-particle ladders outside the model space,

$$G_{ijkl} = V_{ijkl} - \sum_{\alpha\beta} \frac{V_{ij\alpha\beta} G_{\alpha\beta kl}}{\epsilon_\alpha + \epsilon_\beta - \epsilon_i - \epsilon_j + \omega_s}, \quad (1)$$

where ϵ_x are unperturbed (usually kinetic) energies; ij and kl denote orbits in the model space and $\alpha\beta$ orbits outside it, while the starting energy ω_s is treated as a free

parameter. Interestingly, the G matrix approach yields SM interactions that are, up to an overall multiplicative factor of all matrix elements, roughly independent of the NN potential and the starting energy used [5, 7, 8]. The shortcoming of the G matrix is the ill-defined relationship between the starting energy and the model space, thus precluding ab initio calculations.

An alternative to the G matrix approach starts by noting that conventional NN interactions are well-constrained by two-nucleon scattering data only for laboratory energies $E_{\text{lab}} \lesssim 350 \text{ MeV}$. As a consequence, details of nuclear forces are not resolved for relative momenta $k > 2.0 \text{ fm}^{-1}$. Starting from a NN potential, the high-momentum modes can be integrated out in free space using the renormalization group. The resulting low-momentum interaction, called $V_{\text{low } k}$, only has momentum components below a cutoff Λ and evolves with it so that all low-energy two-body observables (phase shifts and deuteron binding energy) are preserved. For $\Lambda \lesssim 2.0 \text{ fm}^{-1}$, all NN potentials that fit the scattering data and include the same long-distance pion physics collapse to a universal $V_{\text{low } k}$ [9]. $V_{\text{low } k}$ defines a new NN interaction without a strong core, that can be directly used in nuclear structure calculations and therefore eliminates all pseudopotential approximations.

When only NN interactions are used, all microscopic approaches have a common problem, related to poor binding and shell formation properties. It reflects in a deteriorating agreement with experiment as the number of particles increases (active particles for the $0\hbar\omega$ SM). This leads to the conclusion that three-nucleon (3N) interactions are necessary. In the case of $V_{\text{low } k}$, it has been shown that chiral 3N forces can be adjusted to remove the cutoff dependence and give perturbative contributions for $\Lambda \lesssim 2.0 \text{ fm}^{-1}$ in light nuclei [11]. In addition, these low-momentum 3N forces drive saturation in nuclear matter [12].

In the first part of this paper, we compare $V_{\text{low } k}$ with G matrices. By studying the cutoff and oscillator frequency

*E-mail: schwenk@indiana.edu

†E-mail: Andres.Zuker@IReS.in2p3.fr

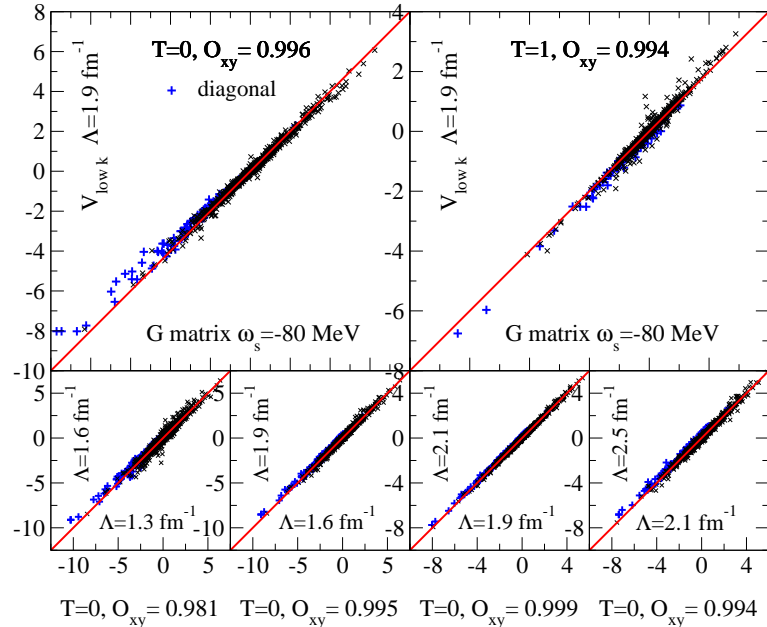


FIG. 1: (Color online) Top: Correlation plots between $V_{\text{low } k}$ and G matrix elements in a restricted space of 4 major shells. The matrix elements V_{rstu}^{JT} are in MeV for $\hbar\omega = 14$ MeV and we have highlighted the diagonal elements. $V_{\text{low } k}$ is derived from the Argonne v_{18} potential and the G matrix is for Idaho A, computed with a rectangular Pauli operator for 4 major shells and starting energy $\omega_s = -80$ MeV [10]. Bottom: Correlation plots between $V_{\text{low } k}$ matrix elements for different cutoffs. To facilitate the comparison, we have rescaled the y -axis set of $V_{\text{low } k}$ matrix elements by $\sigma_{\Lambda_x}/\sigma_{\Lambda_y}$ according to the approximate scaling law Eq. (4). The σ -ratios are from left to right: 1.003, 1.061, 1.050 and 1.111. We find even fewer scatters for the $T = 1$ matrix elements. All O_{AB} given are O_{AB}^T .

dependence of $V_{\text{low } k}$ matrix elements, we demonstrate a universal behavior. A similar behavior exists for G over a reasonable range of starting energies. The second part is devoted to extracting the $V_{\text{low } k}$ monopole Hamiltonian, which is then used to calculate binding energies, as well as single-particle and single-hole spectra on closed-shell nuclei ($cs \pm 1$ spectra). Many features will turn out to be in good agreement with data, and the discrepancies identify what is expected of 3N forces and how they are crucial in heavier systems. Our work shows that the mean-field produced by $V_{\text{low } k}$ is a valuable first approximation that will greatly simplify further perturbative or coupled cluster treatment, and the inclusion of 3N forces.

In Fig. 1, we compare $V_{\text{low } k}$ to G matrix elements in 4 major shells. We find that both $T = 0$ and $T = 1$ matrix elements are very similar. For a quantitative comparison, we define the overlaps of interactions A and B [5, 8]

$$\sigma_{AB}^2 = d_2^{-1} \sum_{rstu\Gamma} [\Gamma] W_{rstuA}^\Gamma W_{rstuB}^\Gamma, \quad (2)$$

where $W_{rstu}^{JT} = V_{rstu}^{JT} - \delta_{rt} \delta_{su} W$ and d_2 is the dimensionality of the two-particle space, each state being counted $[\Gamma] = (2J+1)(2T+1)$ times. Here, the interaction V is referred to its centroid W , defined by $\sum_{rs\Gamma} [\Gamma] W_{rsrs}^\Gamma = 0$. We also introduce normalized overlaps

$$O_{AB} = \frac{\sigma_{AB}^2}{\sigma_A \sigma_B}, \quad (3)$$

W	-1.374	-1.035	-0.802	-0.620	-0.546	-0.463
σ_A	3.288	2.488	1.931	1.500	1.323	1.127
$\hbar\omega$	18.4	13.9	11.0	8.8	7.9	6.9
18.4	1.000	0.992	0.978	0.961	0.952	0.941
13.9	0.992	1.000	0.996	0.987	0.982	0.975
11.0	0.978	0.996	1.000	0.997	0.995	0.990
8.8	0.961	0.987	0.997	1.000	0.999	0.998
7.9	0.952	0.982	0.995	0.999	1.000	0.999
6.9	0.941	0.975	0.990	0.998	0.999	1.000

TABLE I: Centroids W , widths σ_A and overlaps O_{AB} between $V_{\text{low } k}$ matrix elements in 4 major shells for different $\hbar\omega$. $V_{\text{low } k}$ is derived from the Argonne v_{18} potential for $\Lambda = 1.9 \text{ fm}^{-1}$. The values of $\hbar\omega$ correspond approximately from left to right to the double-magic nuclei at $A = 4, 16, 40, 90, 132$ and 208 . G matrices follow the same behavior.

with $\sigma_A = \sigma_{AA}$ and similarly O_{AB}^T for matrix elements with the same T . Interactions that differ at most by a factor σ_A/σ_B have $O_{AB} = 1$. The overlaps between $V_{\text{low } k}$ and the G matrix are $O_{AB} > 0.99$.

Next, we compare $V_{\text{low } k}$ matrix elements for different cutoffs. Over the studied range $\Lambda = 1.3 \dots 3.0 \text{ fm}^{-1}$, we find again very large O_{AB} overlaps, as shown in the bot-

tom panels of Fig. 1. To facilitate the comparison, we have rescaled the y -axis set of $V_{\text{low } k}$ matrix elements by the widths $\sigma_{\Lambda_x}/\sigma_{\Lambda_y}$. Up to this overall factor, we find that $V_{\text{low } k}$ matrix elements are approximately cutoff-independent. From Table I, we find a similar behavior for sets with different $\hbar\omega$ at fixed cutoff. These observations can be combined in an approximate scaling law

$$V_{\text{low } k}^{\Lambda_1, \hbar\omega_1} \approx \frac{\sigma_{\Lambda_1, \hbar\omega_1}}{\sigma_{\Lambda_2, \hbar\omega_2}} V_{\text{low } k}^{\Lambda_2, \hbar\omega_2} \Rightarrow V_{\text{low } k}^{\Lambda, \hbar\omega} \approx \sigma_{\Lambda, \hbar\omega} U, \quad (4)$$

where U_{rstu}^{JT} is a set of two-body matrix elements, approximately independent of Λ and $\hbar\omega$. The decrease of the overlaps as the range of Λ or $\hbar\omega$ increases indicates that different parts of the interaction may scale differently. However, over a fairly wide range, $\sigma_{\Lambda, \hbar\omega}$ follows a simple scaling law,

$$\frac{\sigma_{\Lambda, \hbar\omega_1}}{\sigma_{\Lambda, \hbar\omega_2}} \approx \left(\frac{\hbar\omega_1}{\hbar\omega_2} \right)^\alpha \quad \frac{\sigma_{\Lambda_1, \hbar\omega}}{\sigma_{\Lambda_2, \hbar\omega}} \approx \left(\frac{\Lambda_2}{\Lambda_1} \right)^\beta. \quad (5)$$

Empirically, we have found that the majority of matrix elements scale with $\alpha = 1$ and $\beta = 1/2$. Note that there can be cases when O_{AB} is very large, but the scaling law is not simple. This happens for instance for different starting energies in the G matrices computed from the Bonn potential for $\omega_s = -5 \dots -140$ MeV at fixed $\hbar\omega = 40$ MeV [13], $O_{AB} \gtrsim 0.99$ and σ ranges from 2.22 to 1.85.

The preceding observations suggest that an overall multiplicative factor approximately captures the evolution of the interaction with Λ or $\hbar\omega$. To this list, one would like to add N , the number of $\hbar\omega$ excitations allowed in a model space. As shell model calculations with any microscopic interaction demand very large N to converge to the exact result, it is imperative to define effective interactions for spaces of lower $N\hbar\omega$ (usually $0\hbar\omega$ except for the lightest nuclei). However, for $V_{\text{low } k}$ at $\Lambda \approx 2 \text{ fm}^{-1}$, the particle-particle channel becomes perturbative [12], the scaling laws in Eq. (5) start operating and the $0\hbar\omega$ spaces provide a meaningful first approximation. Therefore, we shall proceed by using the bare $V_{\text{low } k}$ for some very simple $0\hbar\omega$ calculations. The question of N -scaling will be studied in future work, while keeping in mind the evidence from G matrices that perturbative renormalizations amount to multiplicative factors, though different parts of the interaction may scale differently [7, 8].

We start by studying binding energies of closed shell nuclei and $cs \pm 1$ spectra. Unless otherwise noted, in what follows we use $V_{\text{low } k}$ derived from the Argonne v_{18} potential for $\Lambda = 1.9 \text{ fm}^{-1}$. We have checked that, for small cutoffs, the results are practically independent of the precision nuclear force used for $V_{\text{low } k}$.

As a first approximation the $cs \pm 1$ states are single determinants that do not involve configuration mixing and are described by the monopole Hamiltonian H_m . In the oscillator basis, H_m contains a diagonal and a non-diagonal part. The latter is needed for a Hartree-Fock calculation and produces further correlations [5] that will be neglected here.

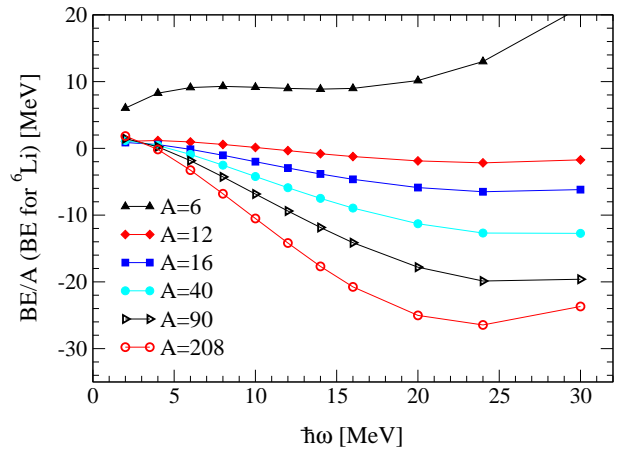


FIG. 2: (Color online) Results for the (negative) binding energies (BE = $\langle H_m^d \rangle$) obtained from Eq. (6) (Coulomb included schematically) by filling lowest oscillator orbits.

In neutron-proton formalism, the diagonal monopole Hamiltonian has a kinetic and a potential part, $H_m^d = K^d + V_m^d$:

$$H_m^d = K^d + \frac{1}{2} \sum_{r_x, s_y} V_{r_x s_y} m_{r_x} (m_{s_y} - \delta_{r_x s_y} \delta_{xy}), \quad (6)$$

where $x, y = n$ or p , and m_{r_x} is the number of particles in orbit r for fluid x . The centroids $V_{r_x s_x}$ are defined in [5]. For an introduction to monopole effects see [14].

In Fig. 2, we show the binding energies of closed shell nuclei. For small $\hbar\omega$, the system is dilute and the interaction behaves as a contact (δ) force, leading to $\alpha = 3/2$ in Eq. (5). We then observe a linear dependence on $\hbar\omega$, $\alpha = 1$, over the range in which the saturation minimum should occur once correlations and 3N forces are included. For large $\hbar\omega$, the interaction effectively becomes long-ranged (α decreases) and the kinetic energy takes over. The binding energies are cutoff dependent without 3N forces. For example, in ^{40}Ca at $\hbar\omega = 12$ MeV, we have $BE/A = 8.24, 5.89$ and 4.52 MeV for $\Lambda = 1.6, 1.9$ (Fig. 2) and 2.1 fm^{-1} respectively. When higher excitations are allowed, the $\hbar\omega$ dependence becomes weaker (as seen for example in [15]), and an exact result will be independent of $\hbar\omega$. Fig. 2 indicates that, for medium-mass and heavy nuclei, 3N interactions should provide a strong repulsion at large $\hbar\omega$.

The case of ^6Li suggests a special behavior in the light nuclei in that a minimum is achieved at a reasonable $\hbar\omega = 14$ MeV, although the total energy is still positive due to the kinetic-potential competition: $\langle K^d \rangle = 88.0$ MeV and $\langle V_m^d \rangle = -81.3$ MeV. Therefore, configuration mixing and 3N contributions should lead to adding 40 MeV to $\langle V_m^d \rangle$, a plausible expectation [4, 15]. Note that a reduction of $V_{\text{low } k}$ to the $0\hbar\omega$ space would demand a factor ≈ 1.4 increase in $\langle V_m^d \rangle$ to achieve the correct result: Again a plausible expectation, suggesting

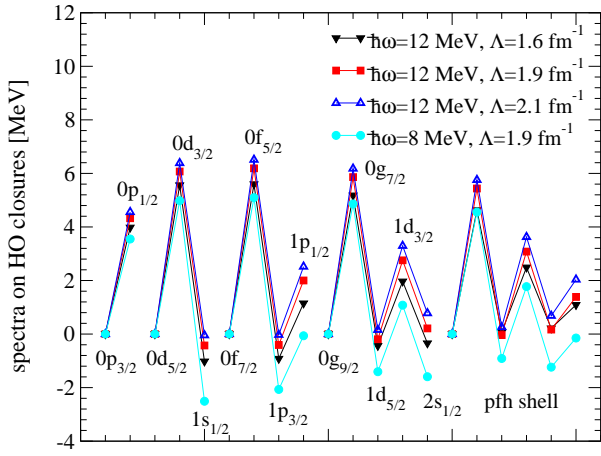


FIG. 3: (Color online) Single-particle spectra on harmonic oscillator closures. Lines (meant to guide the eye) join points belonging to the same major shell. All energies are measured from the largest j subshell in each major shell. We have used Eq. (5) to refer all $V_{\text{low } k}$ matrix elements to $\Lambda = 1.9 \text{ fm}^{-1}$ and rescaled by $(\hbar\omega/\hbar\omega_0)^2 = ((p+2)^2[(p_0+2)^3+3]/(p_0+2)^2[(p+2)^3+3]^2)^2$ (see text), which corresponds to the mass number A appropriate to each major shell with principal quantum number $p+1$. $p_0 = 2$ (4) correspond to the pf (pfh) shell and $\hbar\omega_0 = 12$ (8) MeV.

that for medium-mass and heavy nuclei, the 3N interactions would have to provide an even larger repulsion at large $\hbar\omega$.

To obtain further insight, we study the $cs \pm 1$ spectra. One known problem of an NN-only description is the failure to ensure the $N, Z = 28, 50, 82, \dots$ extruder-intruder magicity [5, 16]. Our results will suggest that this is due to two basic shortcomings, the “ $\mathbf{l} \cdot \mathbf{l}$ ” and “ j_{\max} ” anomalies, that 3N interactions are expected to remedy. These are small effects $\sim A^{1/3}$ compared to the binding energies.

First, we show the single-particle spectra on top of harmonic oscillator closures in Fig. 3. We have scaled all matrix elements to the $\hbar\omega$ corresponding to each major shell. For this we use $\alpha = 2$ in Eq. (5) to comply with the physical imperative that splittings should go asymptotically as $A^{-1/3}$, and we use $\hbar\omega = 35.59A^{1/3}/\langle r^2 \rangle$ MeV, with experimental mean-square radius $\langle r^2 \rangle = 0.943 A^{2/3} (1 + 2/A) \text{ fm}^2$ [17] and $A \approx 2(p+2)^3/3$, where p is the principal oscillator number at the Fermi level. Our results for three values of the cutoff (using the empirical $\beta = 1/2$) and two values of $\hbar\omega$ are shown in Fig. 3. If the scaling laws were perfect, the four patterns should collapse into one. They closely do for different cutoffs but less so for different $\hbar\omega$, indicating that the constant $\alpha = 2$ is too crude.

The splittings between spin-orbit partners in Fig. 3 agree well with experiment, e.g., about 6.0 MeV for both the d orbits in ^{17}O and the f orbits in ^{41}Ca . The sdg and pfh spectra on top of oscillator closures are not di-

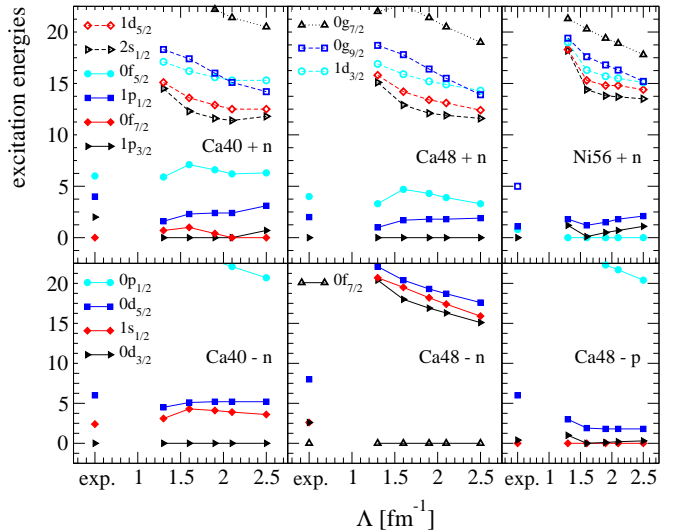


FIG. 4: (Color online) $cs \pm 1$ spectra in the pf region for a wide cutoff range. The experimental $0g_{9/2}$ energy in ^{57}Ni is an estimate.

rectly available but the necessary information can be extracted from the known $cs \pm 1$ spectra up to the Pb region. Our results correspond nicely to those determined empirically [18], e.g., 4.6 MeV for the h orbits as in Fig. 3 for $\hbar\omega = 8 \text{ MeV}$, $\Lambda = 1.9 \text{ fm}^{-1}$. However, what works well in [18] is a combination of one-body $\mathbf{l} \cdot \mathbf{s}$ and $\mathbf{l} \cdot \mathbf{l}$ terms. The latter is attractive beyond the pf shell, thus favoring high l orbits. Fig. 3 shows the opposite: low l orbits are always depressed with respect to the $\mathbf{l} \cdot \mathbf{s}$ standard, and the effect grows bigger in heavier nuclei. This is the $\mathbf{l} \cdot \mathbf{l}$ anomaly.

Splittings for hole states on harmonic oscillator closures are known in ^{15}O and ^{39}Ca (≈ 6 MeV in both). For ^{15}O we obtain about half the observed value, a mean-field result similar to [19]. (Note that this hole splitting is not the same as the particle one in Fig. 3). For ^{39}Ca we are close at 5 MeV, as can be seen in the bottom-left panel of Fig. 4.

This figure compares the $cs \pm 1$ spectra in the pf shell with available data [20] as summarized in [18], where it is shown that a six-parameter monopole Hamiltonian can describe equally well $cs \pm 1$ spectra for $A > 60$ and $A < 60$. The latter are mostly represented by the pf region, which therefore exhibits the basic mechanisms of shell formation (see also [5, 14]). This one-plus-two-body phenomenology reveals what can be explained well by realistic NN potentials, and what cannot must therefore be ascribed to other (presumably 3N) mechanisms. Our task is to establish the distinction.

The results for low-lying pf levels in the upper panel of Fig. 4 are approximately cutoff-independent and the minor discrepancies are cured by SM calculations, which push up the $1p_{3/2}$ orbit in ^{41}Ca , do not change the good spectrum in ^{49}Ca , and also push up by 1 MeV the $0f_{5/2}$

orbit in ^{57}Ni [5, 21]. For the high-lying sdg shell levels, the splittings between spin-orbit partners agree with the empirical values, but the $\mathbf{l} \cdot \mathbf{l}$ anomaly is much stronger than in Fig. 3, and partly responsible for the ~ 10 MeV underbinding of the $0g_{9/2}$ particle orbit in ^{57}Ni . A similar discrepancy shows for the $0f_{7/2}$ hole orbit in ^{47}Ca , underbound by ~ 10 MeV with respect to its sd partners. Such shortcomings are responsible for the failure of NN-only interactions to ensure the $N, Z = 28, 50, 82 \dots$ extruder-intruder closures. This can be directly checked through the standard measures of magicity, the gaps defined as $g(cs, x) = 2BE(cs) - BE(cs + x) - BE(cs - x)$ ($x = n$ or p). The ground state spins are those of Fig. 4. Rounded calculated (experimental) gaps are (in MeV): $g(^{40}\text{Ca}, n) = 13(7)$, $g(^{48}\text{Ca}, p) = 17(6)$, $g(^{48}\text{Ca}, n) = -0.4(5)$ and $g(^{56}\text{Ni}, n) = 0.5(6)$. It follows that extruder-intruder closures are non-existent, and harmonic oscillator closures are too strong. A related problem is that the $0d_{5/2}$ hole orbits in ^{47}Ca and ^{47}K are underbound by ~ 4 MeV with respect to their sd counterparts. On the contrary the $1s_{1/2} - 0d_{3/2}$ splittings are quite good: Although too large by some 1.5 MeV in ^{39}Ca , in ^{47}Ca the splitting is drastically reduced, close to what the data demand, and further reduced in ^{47}K , now very close to experiment.

Thus, we find that when the largest j orbit in a major shell fills, it binds itself and contributes to the binding of the largest j orbits in neighboring shells in a way that NN forces fail to reproduce. This is the j_{\max} anomaly. The necessary intra-shell self-binding to cure it is now well understood in terms of a 3N mechanism [22]. A mechanism to resolve the cross-shell binding problem detected

here remains to be found.

In summary, we have shown that $V_{\text{low } k}$ and G matrix elements are quantitatively similar, but $V_{\text{low } k}$ as a free-space potential is far easier to use in many-body calculations. As a consequence of the similarity, it is possible to build on the successes of the G matrix approach, without the drawbacks due to the ill-defined starting energies and other limitations on the SM by hard potentials. $V_{\text{low } k}$ leads to matrix elements that are approximately cutoff and oscillator frequency independent up to an overall scaling with the width of the interaction. The scaling properties associated to the universal behavior of $V_{\text{low } k}$ have been tested in $cs \pm 1$ spectra. The soft nature of $V_{\text{low } k}$ allows direct monopole estimates of binding energies and $cs \pm 1$ spectra, and in an NN-only description, $V_{\text{low } k}$ reproduces many features of the $cs \pm 1$ spectra. Moreover, our results suggest that, apart from saturation, the main problem that demands a 3N interaction is related to extruder-intruder shell formation.

Finally, it is worth mentioning that ongoing NCSM calculations [23] nicely confirm the validity of our $0\hbar\omega$ explorations. In particular, the saturation patterns for $A = 6, 12, 16$ follow those of Fig. 2 within an overall energy scaling and the spectra of $A = 15, 17$ are the same within few hundred keV. They provide some first suggestions on how nuclear spectroscopy can help to constrain the 3N interactions that prove crucial for a microscopic understanding of nuclear many-body systems.

We thank Hans Feldmeier and Dick Furnstahl for useful discussions. The work of AS is supported by the DOE Grant No. DEFG 0287ER40365 and NSF Grant No. nsf-phy 0244822.

- [1] S. C. Pieper and R. B. Wiringa, Ann. Rev. Nucl. Part. Sci. **51**, 53 (2001).
- [2] S. C. Pieper, R. B. Wiringa, and J. Carlson, Phys. Rev. C **70**, 054325 (2004).
- [3] P. Navrátil, J. P. Vary, and B. R. Barrett, Phys. Rev. C **62**, 054311 (2000).
- [4] P. Navrátil and E. Caurier, Phys. Rev. C **69**, 014311 (2004).
- [5] E. Caurier, G. Martínez-Pinedo, F. Nowacki, A. Poves, and A. P. Zuker, Rev. Mod. Phys. **77**, 427 (2005).
- [6] M. Hjorth-Jensen, T. T. S. Kuo, and E. Osnnes, Phys. Rept. **261**, 126 (1995).
- [7] A. Abzouzi, E. Caurier, and A. P. Zuker, Phys. Rev. Lett. **66**, 1134 (1991).
- [8] M. Dufour and A. P. Zuker, Phys. Rev. C **54**, 1641 (1996).
- [9] S. K. Bogner, T. T. S. Kuo, and A. Schwenk, Phys. Rept. **386**, 1 (2003), for RG details see nucl-th/0111042.
- [10] D. J. Dean and M. Hjorth-Jensen, private communication.
- [11] A. Nogga, S. K. Bogner, and A. Schwenk, Phys. Rev. C **70**, 061002(R) (2004).
- [12] S. K. Bogner, A. Schwenk, R. J. Furnstahl, and A. Nogga, Nucl. Phys. **A763**, 59 (2005).
- [13] M. Hjorth-Jensen, private communication.
- [14] A. P. Zuker, in *Key Topics in Nuclear Structure, Paestum 2004*, edited by A. Covello (World Scientific, 2005).
- [15] L. Coraggio, N. Itaco, A. Covello, A. Gargano, and T. T. S. Kuo, Phys. Rev. C **68**, 034320 (2003).
- [16] E. Pasquini and A. P. Zuker, in *Physics of Medium Light Nuclei, Florence 1977*, edited by P. Blasi (Editrice Compositrice, Bologna, 1978).
- [17] J. Duflo and A. P. Zuker, Phys. Rev. C **66**, 051304(R) (2002).
- [18] J. Duflo and A. P. Zuker, Phys. Rev. C **59**, R2347 (1999).
- [19] S. C. Pieper and V. R. Pandharipande, Phys. Rev. Lett. **70**, 2541 (1993).
- [20] ENSDF section at <http://www.nndc.bnl.gov>.
- [21] F. Nowacki, private communication.
- [22] A. P. Zuker, Phys. Rev. Lett. **90**, 042502 (2003).
- [23] E. Caurier, A. Schwenk, and A. P. Zuker, ongoing work.